

This discussion paper is/has been under review for the journal Natural Hazards and Earth System Sciences (NHESS). Please refer to the corresponding final paper in NHESS if available.

Study of the 2013 Lushan $M = 7.0$ earthquake coseismic ionospheric disturbances

P. Chen^{1,2}, J. J. Chen³, W. Q. Yao¹, and B. Zhang¹

¹College of Geomatics, Xi'an University of Science and Technology, Xi'an 710054, China

²State Key Laboratory of Geodesy and Earth's Dynamics, Wuhan 430077, China

³School of Geodesy and Geomatics, Wuhan University, Wuhan 430079, China

Received: 10 September 2013 – Accepted: 18 September 2013 – Published: 16 October 2013

Correspondence to: P. Chen (chenpeng0123@gmail.com)

Published by Copernicus Publications on behalf of the European Geosciences Union.

NHESSD

1, 5643–5662, 2013

Study of Lushan
earthquake CIDs

P. Chen et al.

Title Page

Abstract

Introduction

Conclusions

References

Tables

Figures

◀

▶

◀

▶

Back

Close

Full Screen / Esc

Printer-friendly Version

Interactive Discussion



Abstract

On 20 April 2013, an earthquake of $M = 7.0$ occurred in Lushan, Sichuan province, China. This paper investigates the coseismic ionospheric anomalies using GPS (Global Positioning System) data from 23 reference stations in Sichuan province that are 5 a part of the Crustal Movement Observation Network of China (CMONOC). The recorded results show that a clear ionospheric anomaly occurred within 15 min after the earthquake near the epicenter, and the occurrence time of the anomalies recorded by various stations is related to the distance from the epicenter. The maximum anomaly 10 is 0.25 TECu, with a 2 min duration and the distance of the recording station to the epicenter is 83 km. Acoustic waves generated by the crustal vertical movement during the earthquake propagate up to the height of the ionosphere lead to the ionospheric anomaly, and the propagation speed of the acoustic wave is calculated as $0.72 \pm 0.04 \text{ km s}^{-1}$ based on the propagation time and propagation distance, consistent with the average speed of sound waves within a 0–450 km atmospheric height.

15 1 Introduction

Seismic events are one of the most serious natural hazards humanity faces, so the study of the mechanisms of earthquakes and seismic anomalies before and after an event has great significance. Ionospheric anomalies caused by the earthquake have been widespread concerned, and many researchers have studied pre-earthquake 20 ionospheric anomalies. The relationships between an earthquake and pre-earthquake ionospheric anomalies have been studied and researchers have obtained regular behaviors of pre-earthquake ionospheric anomalies (Le et al., 2011, 2013; Liu et al., 2000, 2001, 2006, 2009; Pulinets, 2004; Yao et al., 2012a, b; Zhao et al., 2008). In addition, during an earthquake, the atmospheric waves generated by the vertical 25 movement of the ground or sea surface propagate upward and reach the ionosphere inducing the ionospheric electron density anomaly phenomenon known as coseismic

Study of Lushan earthquake CIDs

P. Chen et al.

[Title Page](#)

[Abstract](#)

[Introduction](#)

[Conclusions](#)

[References](#)

[Tables](#)

[Figures](#)

◀

▶

◀

▶

[Back](#)

[Close](#)

[Full Screen / Esc](#)

[Printer-friendly Version](#)

[Interactive Discussion](#)



Study of Lushan earthquake CIDs

P. Chen et al.

[Title Page](#)[Abstract](#)[Introduction](#)[Conclusions](#)[References](#)[Tables](#)[Figures](#)[◀](#)[▶](#)[◀](#)[▶](#)[Back](#)[Close](#)[Full Screen / Esc](#)[Printer-friendly Version](#)[Interactive Discussion](#)

ionospheric disturbances (CIDs) (Calais et al., 1995; Heki and Ping, 2005; Rolland et al., 2011). Various scholars have studied this phenomenon (Calais et al., 1998; Afraimovich et al., 2001; Heki and Ping, 2005; Astafyeva and Heki, 2011; Tsugawa et al., 2011; Saito et al., 2011). Previous technology limitations made it difficult to 5 study the details within CIDs; later, with the emergence of GPS technology, researching CIDs using the ionospheric TEC (total electron content) obtained by GPS technology became a research focus. Astafyeva et al. (2009) studied the 1994 Kurile M8.1 earthquake coseismic ionospheric disturbances and found that there is a correlation between the time of appearance of a CID and its distance to the epicenter, and that 10 CIDs have two different velocity components, the Rayleigh surface wave velocity ($3\text{--}4\text{ km s}^{-1}$) and sound velocity ($0.6\text{--}1.0\text{ km s}^{-1}$), respectively. Liu et al. (2010) found that the 1999 Taiwan Chi-Chi earthquake also caused significant CIDs. Cahyadi et al. (2013) studied the 2007 Bengkulu $M_w = 8.5$ earthquake and the 2005 Nias $M_w = 8.6$ earthquake coseismic ionospheric disturbances, and results indicated that 15 10–16 min after the earthquakes, significant ionospheric disturbances occurred north of the epicenters, and the velocity of the sound waves generated by the seismic events was $\sim 0.7\text{ km s}^{-1}$.

In this paper, using GPS data from the Crustal Movement Observation Network of China (CMONOC) reference stations in Sichuan, we investigate the coseismic 20 ionospheric disturbances after the 20 April 2013 Lushan $M = 7.0$ earthquake and derive the characteristics of the CIDs caused by this event.

2 Data and data processing method

The Lushan $M = 7.0$ earthquake occurred on 20 April 2013 at 00:02:46 UT, from a depth of 14 km, with the epicenter occurring at 30.28°N , 102.95°E , located in the 25 southern section of the Longmen tectonic belt, and was a thrust earthquake; the maximum intensity being of the XI degree.

We use raw GPS data supplied by CMONOC with data sampling rate of 30 s. CMONOC is a high-precision, high spatial and temporal resolution observation network, mainly providing GNSS observations combined with a variety of other techniques, and consists of 260 continuous observation stations and 2000 occasional observation stations primarily used to monitor crustal movement, gravity field, tropospheric water vapor content, and ionospheric ion concentration related to the Chinese mainland.

5 GPS satellites transmit dual-frequency signals of 1575.42 MHz and 1227.60 MHz, corresponding to wavelengths of 19.03 cm and 24.42 cm, respectively. Since the ionosphere is a dispersive medium, GPS signals suffer an ionospheric delay dependent 10 on the signal frequency; therefore, using dual-frequency phase observations can provide the total electron content STEC_φ along the GPS signal propagation path. During CIDs detection and analysis only the relative change of the STEC, STEC_φ, is determined with high accuracy and has been considered a suitable method for the 15 detection of CIDs. The formula of the STEC calculation using GPS dual frequency phase observations can be written as (Calais et al., 1995):

$$\text{STEC}_\varphi = \frac{f_1^2 f_2^2}{40.3 \cdot (f_1^2 - f_2^2)} \cdot [(\lambda_1 \varphi_1 - \lambda_2 \varphi_2) + N + \varepsilon_\varphi]. \quad (1)$$

where f_1 and f_2 are the GPS carrier frequencies; φ_1 and φ_2 are dual-frequency carrier phase measurements of the two frequencies (in units of cycle); λ_1 and λ_2 are the GPS carrier wavelengths; N is the ambiguity of phase measurements; ε_φ is the 20 observation noise. Currently, the carrier phase measurement accuracy of a geodesy type GPS receiver is 0.2–0.3 mm, and if we ignore the impact of ambiguity, then the accuracy of STEC_φ is 0.0027–0.0040 TECu, well suited for detecting small ionospheric disturbances.

25 GPS satellites have relatively smooth orbits, so if a station continuously tracks the same satellite, the obtained STEC should also be relatively smooth under quiet

[Title Page](#)

[Abstract](#)

[Introduction](#)

[Conclusions](#)

[References](#)

[Tables](#)

[Figures](#)

[◀](#)

[▶](#)

[◀](#)

[▶](#)

[Back](#)

[Close](#)

[Full Screen / Esc](#)

[Printer-friendly Version](#)

[Interactive Discussion](#)



Study of Lushan earthquake CIDs

P. Chen et al.

[Title Page](#)[Abstract](#)[Introduction](#)[Conclusions](#)[References](#)[Tables](#)[Figures](#)[◀](#)[▶](#)[◀](#)[▶](#)[Back](#)[Close](#)[Full Screen / Esc](#)[Printer-friendly Version](#)[Interactive Discussion](#)

ionosphere conditions, but fluctuations in the TEC occur a short time after an earthquake (the CIDs caused by the earthquake). However, the change rate of the STEC is large and it is difficult to detect any slight anomalies directly through STEC. For this reason, Liu et al. (2004) proposed an ionospheric anomaly detection method

5 through a single difference operation of the TEC, $d\text{TEC}$, but there are still large fluctuations that mask small anomalies using this method. We propose differencing the TEC again to obtain $d^2\text{TEC}$, where the change of $d^2\text{TEC}$ is more stable and allows easier detection of minuscule fluctuations in the ionosphere. $d\text{TEC}$, and $d^2\text{TEC}$ are calculated by Eq. (2):

$$10 \quad \begin{aligned} d\text{TEC}_i &= \text{TEC}_{i+1} - \text{TEC}_i \\ d\text{TEC}_{i+1} &= \text{TEC}_{i+2} - \text{TEC}_{i+1} \\ d^2\text{TEC}_i &= d\text{TEC}_{i+1} - d\text{TEC}_i \end{aligned} \quad (2)$$

Using a single layer ionosphere assumption in data processing, namely that all electrons in the ionosphere are concentrated in an infinitely-thin layer at a certain height (450 km in this article). The intersection point of the receiver and satellite connection path and the thin layer is named the Ionospheric Pierce Point IPP, and the projection point of the IPP on the ground is named the Sub Ionospheric Point, SIP. The positional relationships among the receiver, satellite, IPP and SIP are shown in Fig. 1.

15 The IPP coordinate when a CID occurs based on the CID's time of occurrence and the distance between the epicenter and the IPP is used to calculate the propagation velocity of atmospheric seismic waves generated by an earthquake.

20 Figure 2 shows the epicenter of the Lushan earthquake and the distribution map of the 23 CMONOC GPS continuous tracking stations in Sichuan province discussed in this paper, where the blue star denotes the location of the epicenter. As can be seen from the figure, the GPS continuous tracking stations are very close to the epicenter, where the nearest station, SCTQ, is only 55 km from the epicenter, and the furthest station, SCPZ, is only 467 km from the epicenter. The high distribution density of the tracking stations can effectively capture any weak ionospheric anomalies.

3 Analysis

Satellites and receivers formed a dense IPP distribution around the epicenter, but only a small number of IPPs in this region were useful when the CID reached the height of the ionosphere, so only a small number of satellites were able to monitor

5 the CID. Figure 3 shows the STEC time series diagram using dual-frequency phase observations from nine PRN15 satellite tracking stations near the epicenter during 00:00–01:00 UT, 20 April. The figure shows that the STEC is smoother in the quiet period, but produces short-term fluctuations as the seismic waves spread to the height of the ionosphere, and later return to normal. STEC obtained by stations SCYX, SCYY,
10 SCXD, SCMN, SCML, and SCJL indicate ionospheric anomalies occurred within 10 to 13 min after the earthquake, and SCYX, SCXD and SCMN recorded the most significant anomalies. The distances from the abnormal occurrence locations to the epicenter were 43.7, 59.9, and 46.2 km, and the amplitudes of the anomalies were 0.09, 0.08, and 0.09 TECu, all with durations of 90 s.

15 Figure 4a and b show the time series curves calculated by $d\text{TEC}$ and $d^2\text{TEC}$ during 00:00–01:00 UT on 20 April 2013, respectively. The figure indicates that single difference can eliminate the trend term of STEC, and $d\text{TEC}$ varies within ± 0.1 TECu, but there are still obvious fluctuations. Differencing $d\text{TEC}$ again to obtain $d^2\text{TEC}$, more stable curves are obtained, and fluctuations are very close to zero
20 under quiet conditions, but obvious fluctuations appear when the CID occurs. The double differencing method we propose is very suitable for the detection of coseismic ionospheric disturbances.

25 Figure 5 shows the STEC and $d^2\text{TEC}$ time series of the SCJU tracking station and PRN21 observation station. Figure 5a shows that very significant ionosphere disturbance occurred within 10 min after the earthquake, first appearing as positive anomalies with a maximum amplitude of 0.1 TECu, and then became negative anomalies that lasted approximately two min before the STEC returned to normal. It can be seen from Fig. 5b that the $d^2\text{TEC}$ curve is close to zero and relatively stable in

[Title Page](#)

[Abstract](#)

[Introduction](#)

[Conclusions](#)

[References](#)

[Tables](#)

[Figures](#)

◀

▶

◀

▶

[Back](#)

[Close](#)

[Full Screen / Esc](#)

[Printer-friendly Version](#)

[Interactive Discussion](#)



Study of Lushan earthquake CIDs

P. Chen et al.

[Title Page](#)[Abstract](#)[Introduction](#)[Conclusions](#)[References](#)[Tables](#)[Figures](#)[◀](#)[▶](#)[◀](#)[▶](#)[Back](#)[Close](#)[Full Screen / Esc](#)[Printer-friendly Version](#)[Interactive Discussion](#)

ionospheric quiet conditions, with fluctuations within ± 0.05 TECu, and the curve jumps sharply when the ionosphere disturbance induced by the earthquake occurs (shown in the red circle), with a maximum amplitude of over 0.25 TECu.

Table 1 shows the CIDs occurrence time, the geodetic coordinates of the IPPs and the calculated atmospheric acoustic propagation velocity calculated from 7 tracking stations that detected the CIDs. From the table, the calculated velocity of wave propagation by the different stations varied within $0.63\text{--}0.77\text{ km s}^{-1}$ with an average of 0.72 km s^{-1} , and the standard deviation was 0.06 km s^{-1} . This result is very close to the $0.69 \pm 0.04\text{ km s}^{-1}$ calculated by Cahyadi et al. (2013) for the 2007 Bengkulu earthquake.

Figure 6 shows the location map of the ionospheric anomaly, where the star denotes the epicenter, the triangle denote the tracking stations that detected the CIDs, the blue curves are the SIP trajectory of a PRN15 satellite, and SCJL, SCMN, SCYX, SCXD, SCML, and SCYY are the 6 tracking stations during 00:00–01:00 UT, the green curve denotes the PRN21 satellite and SCJU, and the asterisk indicates the SIP location when the coseismic ionospheric disturbances occurred. It can be seen that due to the relatively small magnitude of the earthquake, the ionospheric disturbances caused by the earthquake were limited to a small area near the epicenter, and the maximum distance of the CIDs from the epicenter was only 133.6 km, while there were no obvious ionospheric disturbances at further distances.

Figure 7 shows the relationships among $d^2\text{TEC}$, CIDs occurrence time, and the distance to the epicenter. The figure shows that under quiet conditions the $d^2\text{TEC}$ is very close to zero, but shows a disturbance with amplitude of $-0.15\text{--}0.25$ TECu when the CIDs occur. The detection occurrence time of the CIDs varies with the distance to the epicenter, and the best connection line shown as the solid red line represents the average speed of the seismic wave during propagation from the epicenter to the IPPs and is almost the same as the $0.72 \pm 0.06\text{ km s}^{-1}$ calculated in Table 1.

Figure 8 shows the relationship between the propagation velocity of the acoustic wave and its height from the ground within 0–450 km. The propagation velocity of

Study of Lushan earthquake CIDs

P. Chen et al.

[Title Page](#)[Abstract](#)[Introduction](#)[Conclusions](#)[References](#)[Tables](#)[Figures](#)[◀](#)[▶](#)[◀](#)[▶](#)[Back](#)[Close](#)[Full Screen / Esc](#)[Printer-friendly Version](#)[Interactive Discussion](#)

the acoustic wave is about 980 m s^{-1} at the ionosphere height, much larger than the propagation velocity of 320 m s^{-1} at ground level. The propagation velocity of sound has small variation under a 100 km height; the velocity decreases with increasing height within 0–20 km and 50–85 km height ranges, and within 20–50 km the velocity increases with increasing height. The propagation velocity increases rapidly with increasing height from 100–400 km and essentially remains constant from 400–450 km. According to the figure, at different heights from the ground to the ionospheric height, the average acoustic wave propagation velocity is 710.03 m s^{-1} , and is very close to the Lushan earthquake wave average propagation velocity of 0.72 km s^{-1} calculated in this paper, indicating that CIDs are indeed caused by sound waves generated by earthquakes that propagate to the ionosphere height, and also indicates that the methods and results applied in this article are valid.

4 Conclusions

We investigate the 20 April 2013 Lushan $M = 7.0$ earthquake coseismic ionospheric anomalies. The STEC data obtained by CMONOC GPS observations is analyzed, and the results show that the ionospheric anomalies occurred near the epicenter within 10–13 min after the earthquake. Through the studies of the epicenter's location of CIDs, and the propagation velocity of the seismic waves generated by the earthquake, the following conclusions apply:

1. The magnitude and duration of CIDs caused by this earthquake are relatively small, and the CIDs locations are very close to the epicenter due to the relatively small magnitude of the earthquake.

2. The results show that seismic waves propagate from the ground to the height of the ionosphere with an average velocity of $0.72 \pm 0.06 \text{ km s}^{-1}$, a very close result to the average velocity of sound wave propagation (710 m s^{-1}) within a 0–450 km atmospheric height, indicating that CIDs are indeed caused by sound waves that are generated by earthquakes and propagate up to the ionosphere.

However, we present a preliminary study of the CIDs after the Lushan earthquake, and examines only the component caused by the spread of acoustic velocity waves. Further studies to determine whether higher speed transmission components exist during a seismic event should be carried out.

5 **Acknowledgements.** Thanks to CMONOC to provide the GPS data. The project supported by State Key Laboratory of Geodesy and Earth's Dynamics Fund (SKLGED2013-4-10-EB), the Surveying and Mapping Foundation Research Fund Program, State Bureau of Surveying and Mapping (12-01-07) and Xi'an University of Science and Technology cultivation fund (201204).

References

10 Afraimovich, E. L., Perevalova, N. P., Plotnikov, A. V., and Uralov, A. M.: The shock-acoustic waves generated by earthquakes, *Ann. Geophys.*, 19, 395–409, doi:10.5194/angeo-19-395-2001, 2001.

15 Astafyeva, E. and Heki, K.: Vertical TEC over seismically active region during low solar activity, *J. Atmos. Sol.-Terr. Phy.*, 73, 1643–1652, 2011.

20 Astafyeva, E., Heki, K., Kiryushkin, V., Afraimovich, E., and Shalimov, S.: Two-mode long-distance propagation of coseismic ionosphere disturbances, *J. Geophys. Res.*, 114, A10307, doi:10.1029/2008JA013853, 2009.

25 Astafyeva, E., Shalimov, S., Olshanshaya, E., and Lognonné, P.: Ionospheric response to earthquakes of different magnitudes: larger quakes perturb the ionosphere stronger and longer, *Geophys. Res. Lett.*, 40, 1675–1681, doi:10.1002/grl.50398, 2013.

30 Cahyadi, M. N. and Heki, K.: Ionospheric disturbances of the 2007 Bengkulu and the 2005 Nias earthquakes, Sumatra, observed with a regional GPS network, *J. Geophys. Res.*, 118, 1777–1787, doi:10.1002/jgra.50208, 2013.

35 Calais, E. and Minster, J. B.: GPS detection of ionospheric perturbations following the January 17, 1994, Northridge earthquake, *Geophys. Res. Lett.*, 22, 1045–1048, 1995.

40 Calais, E., Bernard Minster, J., Hofton, M., and Hedlin, M.: Ionospheric signature of surface mine blasts from Global Positioning System measurements, *Geophys. J. Int.*, 132, 191–202, 1998.

[Title Page](#)

[Abstract](#)

[Introduction](#)

[Conclusions](#)

[References](#)

[Tables](#)

[Figures](#)

◀

▶

◀

▶

[Back](#)

[Close](#)

[Full Screen / Esc](#)

[Printer-friendly Version](#)

[Interactive Discussion](#)



Study of Lushan earthquake CIDs

P. Chen et al.

Choosakul, N., Saito, A., Iyemori, T., and Hashizume, M.: Excitation of 4-min periodic ionospheric variations following the great Sumatra-Andaman earthquake in 2004, *J. Geophys. Res.*, 114, A10313, doi:10.1029/2008JA013915, 2009.

Heki, K.: Ionospheric electron enhancement preceding the 2011 Tohoku-Oki earthquake, *Geophys. Res. Lett.*, 38, L17312, doi:10.1029/2011GL047908, 2011.

Heki, K. and Ping, J.: Directivity and apparent velocity of the coseismic ionospheric disturbances observed with a dense GPS array, *Earth Planet. Sc. Lett.*, 236, 845–855, 2005.

Kamogawa, M. and Kakinami, Y.: Is an ionospheric electron enhancement preceding the 2011 Tohoku-Oki earthquake a precursor?, *J. Geophys. Res.-Space*, 118, 1751–1754, doi:10.1002/jgra.50118, 2013.

Kunitsyn, V. E., Nesterov, I. A., and Shalimov, S. L.: Japan megathrust earthquake on March 11, 2011: GPS-TEC evidence for ionospheric disturbances, *JETP Lett.+*, 94, 616–620, 2011.

Le, H., Liu, J. Y., and Liu, L.: A statistical analysis of ionospheric anomalies before 736 M6.0+ earthquakes during 2002–2010, *J. Geophys. Res.*, 116, A02303, doi:10.1029/2010JA015781, 2011.

Le, H., Liu, L., Liu, J. Y., Zhao, B., Chen, Y., and Wan, W.: The ionospheric anomalies prior to the M9.0 Tohoku-Oki earthquake, *J. Asian Earth Sci.*, 62, 476–484, 2013.

Liu, J. Y., Chen, Y. I., Pulinets, S. A., Tsai, Y. B., and Chuo, Y. J.: Seismo-ionospheric signatures prior to $M \geq 6.0$ Taiwan earthquakes, *Geophys. Res. Lett.*, 27, 3113–3116, 2000.

Liu, J. Y., Chen, Y. I., Chuo, Y. J., and Tsai, H. F.: Variations of ionospheric total electron content during the Chi-Chi earthquake, *Geophys. Res. Lett.*, 28, 1383–1386, 2001.

Liu, J. Y., Lin, C. H., Tsai, H. F., and Liou, Y. A.: Ionospheric solar flare effects monitored by the ground-based GPS receivers: Theory and observation, *J. Geophys. Res.*, 109, A01307, doi:10.1029/2003JA009931, 2004.

Liu, J. Y., Chen, Y. I., Chuo, Y. J., and Chen, C. S.: A statistical investigation of preearthquake ionospheric anomaly, *J. Geophys. Res.*, 111, A05304, doi:10.1029/2005JA011333, 2006.

Liu, J. Y., Chen, Y. I., Chen, C. H., Liu, C. Y., Chen, C. Y., Nishihashi, M., and Lin, C. H.: Seismoionospheric GPS total electron content anomalies observed before the 12 May 2008 Mw7.9 Wenchuan earthquake, *J. Geophys. Res.*, 114, A04320, doi:10.1029/2008JA013698, 2009.

Liu, J. Y., Tsai, H. F., Lin, C. H., Kamogawa, M., Chen, Y. I., Lin, C. H., Huang, B. S., Yu, S. B., and Yeh, Y. H.: Coseismic ionospheric disturbances triggered by the Chi-Chi earthquake, *J. Geophys. Res.*, 115, A08303, doi:10.1029/2009JA014943, 2010.

[Title Page](#)[Abstract](#)[Introduction](#)[Conclusions](#)[References](#)[Tables](#)[Figures](#)[◀](#)[▶](#)[◀](#)[▶](#)[Back](#)[Close](#)[Full Screen / Esc](#)[Printer-friendly Version](#)[Interactive Discussion](#)

Study of Lushan earthquake CIDs

P. Chen et al.

Pulinets, S. A. and Boyarchuk, K. A.: Ionospheric Precursors of Earthquakes, Springer, Berlin, New York, 2004.

Rolland, L. M., Lognonné, P., Astafyeva, E., Kherani, E. A., Kobayashi, N., Mann, M., and Munekane, H.: The resonant response of the ionosphere imaged after the 2011 off the Pacific coast of Tohoku Earthquake, *Earth Planets Space*, 63, 853–857, 2011.

Saito, A., Tsugawa, T., Otsuka, Y., Nishioka, M., Iyemori, T., Matsumura, M., and Choosakul, N.: Acoustic resonance and plasma depletion detected by GPS total electron content observation after the 2011 off the Pacific coast of Tohoku Earthquake, *Earth Planets Space*, 63, 863–867, 2011.

10 Tsugawa, T., Saito, A., Otsuka, Y., Nishioka, M., Maruyama, T., Kato, H., and Murata, K. T.: Ionospheric disturbances detected by GPS total electron content observation after the 2011 off the Pacific coast of Tohoku Earthquake, *Earth Planets Space*, 63, 875–879, 2011.

Yao, Y. B., Chen, P., Wu, H., Zhang, S. and Peng, W. F.: Analysis of ionospheric anomalies before the 2011 Mw9.0 Japan earthquake, *Chinese Sci. Bull.*, 57, 355–365, 2012a.

15 Yao, Y. B., Chen, P., Zhang, S., Chen, J. J., Yan, F., and Peng, W. F.: Analysis of pre-earthquake ionospheric anomalies before the global $M = 7.0+$ earthquakes in 2010, *Nat. Hazards Earth Syst. Sci.*, 12, 575–585, doi:10.5194/nhess-12-575-2012, 2012b.

Zhao, B., Wang, M., Yu, T., Wan, W., Lei, J., Liu, L., and Ning, B.: Is an unusual large enhancement of ionospheric electron density linked with the 2008 great Wenchuan earthquake?, *J. Geophys. Res.*, 113, A11304, doi:10.1029/2008JA013613, 2008.

20

Title Page	
Abstract	Introduction
Conclusions	References
Tables	Figures
◀	▶
◀	▶
Back	Close
Full Screen / Esc	
Printer-friendly Version	
Interactive Discussion	



Study of Lushan
earthquake CIDs

P. Chen et al.

Table 1. Occurrence moment of the CIDs, geodetic coordinates of IPPs, and wave propagation velocity from 7 tracking stations that detected the 20 April 2013 CIDs.

Station	Occurrence time (UT)	Latitude (degree)	Longitude (degree)	Propagation velocity (km s^{-1})
SCJL	0:13:00	30.4800	102.4500	0.76
SCJU	0:13:00	30.5027	102.1339	0.77
SCML	0:15:00	29.5700	102.2900	0.65
SCMN	0:13:30	29.8799	103.0881	0.72
SCXD	0:13:30	29.8477	103.3309	0.73
SCYX	0:13:00	30.1476	103.3887	0.76
SCYY	0:15:30	29.1395	102.5238	0.63

[Title Page](#)[Abstract](#)[Introduction](#)[Conclusions](#)[References](#)[Tables](#)[Figures](#)[◀](#)[▶](#)[◀](#)[▶](#)[Back](#)[Close](#)[Full Screen / Esc](#)[Printer-friendly Version](#)[Interactive Discussion](#)

Study of Lushan
earthquake CIDs

P. Chen et al.

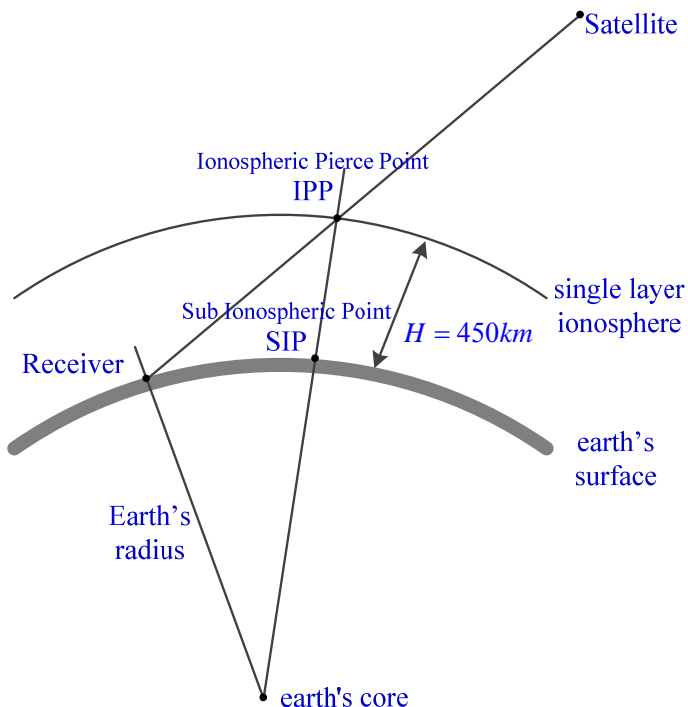


Fig. 1. Receiver, satellite, IPP and SIP positional relationships.

Study of Lushan earthquake CIDs

P. Chen et al.

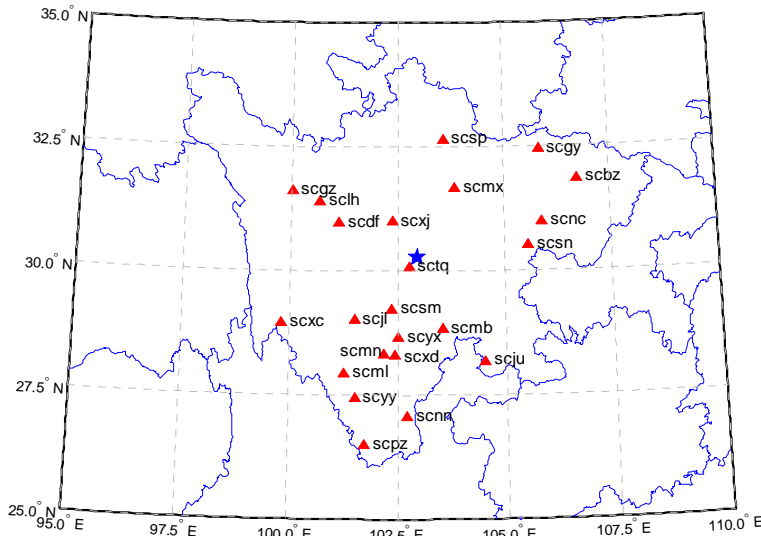


Fig. 2. Location map of the 20 April 2013 earthquake epicenter and existing CMONOC GPS continuous tracking stations in Sichuan province.

Title Page	
Abstract	Introduction
Conclusions	References
Tables	Figures
◀	▶
◀	▶
Back	Close
Full Screen / Esc	
Printer-friendly Version	
Interactive Discussion	

Discussion Paper | Study of Lushan earthquake CIDs

P. Chen et al.

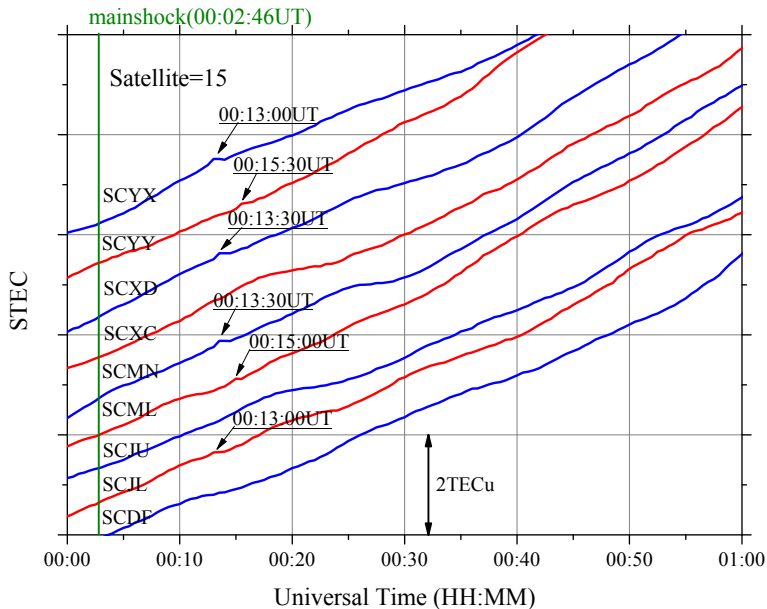


Fig. 3. Nine stations obtained PRN15 satellite STEC time series curves at 00:00–01:00 UT, 20 April. In the figure, the green line represents the moment of the earthquake, and the time stamps represent the moment obvious disturbances were detected by the tracking stations.

- [Title Page](#)
- [Abstract](#) [Introduction](#)
- [Conclusions](#) [References](#)
- [Tables](#) [Figures](#)
- [◀](#) [▶](#)
- [◀](#) [▶](#)
- [Back](#) [Close](#)
- [Full Screen / Esc](#)
- [Printer-friendly Version](#)
- [Interactive Discussion](#)

Study of Lushan earthquake CIDs

P. Chen et al.

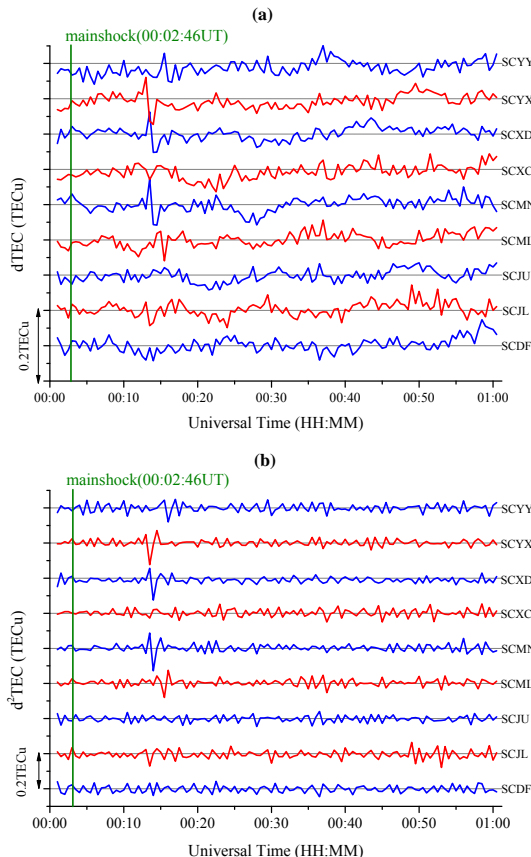


Fig. 4. $d\text{TEC}$ and $d^2\text{TEC}$ PRN15 time series curves of 9 GPS tracking stations during 00:00–01:00 UT, 20 April 2013.

Study of Lushan
earthquake CIDs

P. Chen et al.

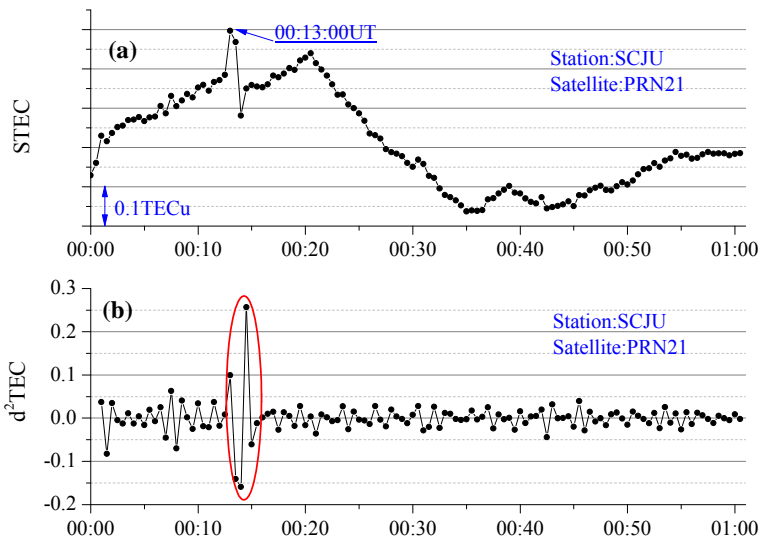


Fig. 5. The STEC and $d^2\text{TEC}$ time series curves obtained from SCJU and PRN21 data collected from 00:00–01:00 UT on 20 April 2013.

Study of Lushan earthquake CIDs

P. Chen et al.

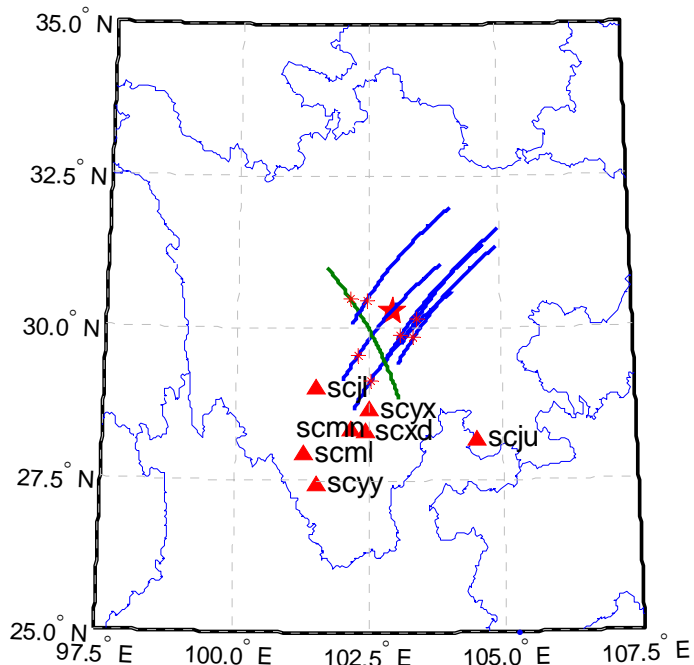


Fig. 6. Map of the CID detection stations and satellites.

[Title Page](#)[Abstract](#)[Introduction](#)[Conclusions](#)[References](#)[Tables](#)[Figures](#)[◀](#)[▶](#)[◀](#)[▶](#)[Back](#)[Close](#)[Full Screen / Esc](#)[Printer-friendly Version](#)[Interactive Discussion](#)

Study of Lushan earthquake CIDs

P. Chen et al.

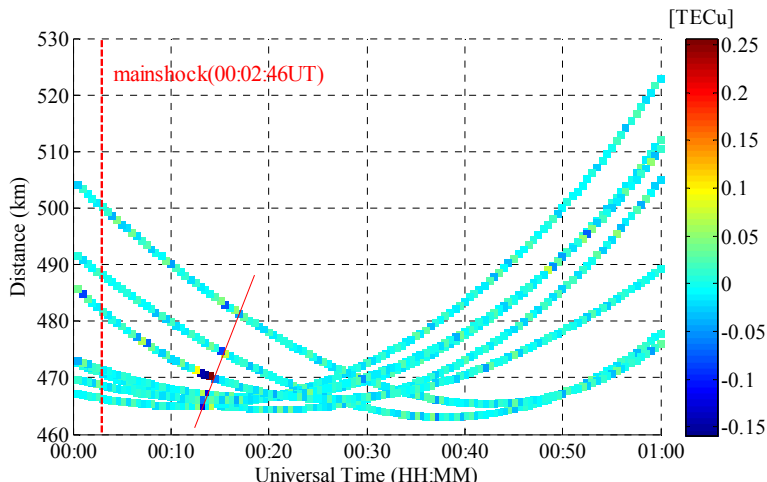


Fig. 7. Relationships among $d^2\text{TEC}$, the occurrence moment of the CIDs and the distance from the epicenter. UT time is the abscissa, the distance between an IPP and the epicenter is the vertical coordinate, $d^2\text{TEC}$ is described with different colors (the colored bar), the red dotted line indicates the earthquake moment, and the thin red solid line indicates the connection line of the maximum values of $d^2\text{TEC}$.

Study of Lushan earthquake CIDs

P. Chen et al.

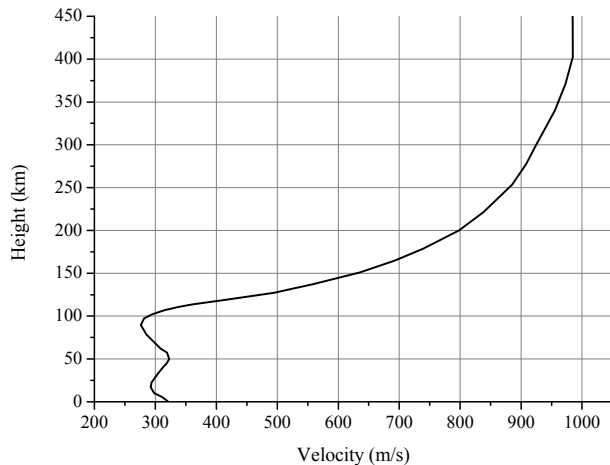


Fig. 8. Wave transmission velocity diagram within 0–450 km from the ground (Calais et al., 1998).

- [Title Page](#)
- [Abstract](#) [Introduction](#)
- [Conclusions](#) [References](#)
- [Tables](#) [Figures](#)
- [◀](#) [▶](#)
- [◀](#) [▶](#)
- [Back](#) [Close](#)
- [Full Screen / Esc](#)
- [Printer-friendly Version](#)
- [Interactive Discussion](#)

